THE JOURNAL OF PHYSICAL CHEMISTRY A
A JOURNAL OF THE AMERICAN CHEMICAL SOCIETY

pubs.acs.org/JPCA

Article

ReaxFF Force Field Development for Gas-Phase hBN Nanostructure Synthesis

Aditya Lele, Predrag Krstic, and Adri C. T. van Duin*

Cite This: J. Phys. Chem. A 2022, 126, 568−582

Read Online

ACCESS | Metrics & More | Article Recommendations | Supporting Information

ABSTRACT: Two-dimensional (2D) hexagonal boron nitride materials are isomorphs of carbon nanomaterials and hold promise for electronics applications owing to their unique properties. Despite the recent advances in synthesis, the current production capacity for boron nitride (BN) nanostructures is far behind that for carbon-based nanostructures. Understanding the growth mechanism of BN nanostructures through modeling and experiments is key to improving this situation. In the current work, we present the development of a ReaxFF-based force field capable of modeling the gas-phase chemistry important for the chemical vapor deposition (CVD) synthesis process. This force field is parameterized to model the boron nitride nanostructure (BNNS) formation in the gas phase using BN and HBNH as precursors. Our ReaxFF simulations show that BN is the best of these two precursors in terms of quality and the size of BNNSs. The BN precursors lead to the formation of closed BNNSs. However, BNNSs are replaced with complex polymeric structures at temperatures of 2500 K and higher due to entropic effects. Compared to the BN precursors, the HBNH precursors form relatively small, flat, and low-quality BNNSs, but this structure is less affected by temperature. Additives like H_2 significantly affect the BNNS formation by preventing closed BNNS formation. Our results show the ReaxFF capability in predicting the BN gas-phase chemistry and BNNS formation, thus providing key insights for experimental synthesis.

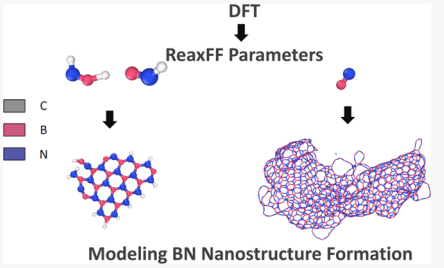

1. INTRODUCTION

Two-dimensional (2D) hexagonal boron nitride (hBN) is considered one of the most promising 2D materials. hBN, an isomorph of graphene, has widely been used as an electric insulator and heat-resistant material for many decades.[1] With its excellent thermal stability, chemical inertness, and unique optoelectrical properties, it is considered to be an ideal candidate for integration with other 2D materials. 2D-hBN is formed by an sp^2 hybridized network of six-membered rings made of alternate B and N atoms similar to that of graphene formed with six-membered rings of carbon.[2]

Being a 2D material with attractive properties, the synthesis of hBN has received significant research interest. The chemical vapor deposition (CVD) technique is the most thoroughly explored and promising method for the large-scale production of hBN.[3] In CVD, a variety of precursors such as BF_3/NH_3, BCl_3/NH_3, borazine, and B_2H_6/NH_3 are used to deposit 2D-hBN on a substrate. The precursors containing just B, N, and H atoms are attractive because they do not produce highly toxic byproducts such as BF_3 or BCl_3.[3] While the C-based precursors do not have this issue, they could lead to carbon contamination in 2D-hBN.[4] The CVD growth of hBN is affected by the type of precursor, ambient gas conditions (temperature, pressure), and the substrate. These variables affect the quality as well as the growth rate of 2D-hBN.

BN nanostructures (BNNS), especially BN nanotubes (BNNT), can also be synthesized using other methods such as arc discharge, laser ablation methods, chemical or mechanical exfoliation, etc.[5−9] These synthesis techniques typically use high temperatures, pressures, and atomic sources of B (B clusters) and N (N_2 gas) to synthesize BNNTs commercially.[10] Previous studies have suggested that the introduction of hydrogen in these environments could enhance BNNS formation by producing B−N−H species.[5,6] The presence of H not only enhances the production of c-BN at ambient pressure[11] but also enhances the production of h-BN by preventing closing h-BN structures into cocoons.[12] The production rate for BN nanostructures has not reached the levels attained by carbon-based nanostructures despite the recent advances in synthesis.[10] Understanding the growth mechanism of BN nanostructures through modeling and experiments is key to improving this situation. On the modeling front, Liu et al.[13] studied the nucleation and formation of hBN on a Ni surface using a combination of density functional theory (DFT) and reactive molecular dynamics. McLean et al.[14] studied the synthesis of BNNTs during Ni-catalyzed chemical vapor deposition (CVD) of ammonia borane using ReaxFF. Their work highlighted the

Received: November 8, 2021
Revised: January 3, 2022
Published: January 20, 2022

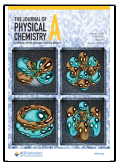

role of Ni in the synthesis process including Ni-catalyzed production of H_2 following B−H bond activation, the oligomerization of surface-bound BN chains, and the facilitation of homoelemental (B−B, N−N) bond cleavage by the Ni catalyst to afford ring closure.

Krstic et al.[15] used quantum-classical molecular dynamics (QCMD) using the density functional tight-binding (DFTB) quantum method to simulate the synthesis of BNNS in a hot, high-pressure gas volume. Here, DFTB is implemented through the divide-and-conquer (DC) linear scaling algorithm in DC−DFTB-K code, which facilitates application to large systems at ns times. They studied the formation of BNNS using various precursors including BN, BN+H, HBNH, and $B_3N_3H_6$. Barsukov et al.[16] modeled the chemical pathways of formation for boron nitride nanotube (BNNT) precursors during high-temperature synthesis in a B/N_2 mixture using quantum chemistry, quantum-classical molecular dynamics, thermodynamic, and kinetic approaches. The previous ReaxFF studies[13,14] focused on studying the growth mechanisms for BNNS on catalytic surfaces. The more recent quantum-classical molecular dynamics simulations[15] focus on the high-temperature gas-phase synthesis of BNNS from a range of precursors. None of the existing computational studies focus on the synthesis of BNNS with precursors such as B_2H_6/NH_3. Additionally, QCMD methods are limited by their computational requirements compared to the classical reactive MD methods such as ReaxFF. For example, ReaxFF is roughly 20 times faster and shows better scaling than DFTB for identical systems.[17]

The aim of this work is twofold. First, we present the development of a ReaxFF-based force field capable of modeling the gas-phase chemistry important for the CVD gas-phase synthesis process of BNNS formation. The second target is to demonstrate the modeling capabilities of the force field. Hence, the work is arranged as follows: the next section gives a summary of the computational methods used in this work. In the Results section, we first discuss the force field development process, followed by a discussion of some key gas-phase reactions. Thereafter, we discuss the results of the synthesis of BNNS using BN and HBNH as precursors. We also discuss the effect of thermodynamic variables (temperature and pressure) and additives on the BNNS formation process. Afterward, we compare ReaxFF results presented in this work with those performed using DFTB.[15] In the end, the conclusions highlight the key takeaways from the force field development and the potential application areas.

2. SIMULATION DETAILS

2.1. ReaxFF Reactive Molecular Dynamics Method. The ReaxFF reactive force field-based MD is a computational tool for atomistic-scale simulations of complex reactive systems.[18,19] The ReaxFF reactive force field is mainly trained against quantum mechanics (QM) data, and the ReaxFF methodology describes chemically reactive events through the interatomic potential within a bond-order formalism, thus describing the bond formation and breaking without expensive QM calculations. Since ReaxFF requires a significantly lower computational cost than QM, it can simulate reaction processes over a longer time (≫1 ns) and larger sizes (≫10 000 atoms). Additionally, ReaxFF does not require any user intuition for possible reaction processes beyond its initial training, thus enabling it to simulate complex reactive systems.

Briefly, in the ReaxFF method, reactive events are described through a bond-order concept,[20] where the bond order is calculated directly from an interatomic distance using an empirical formula that contains the single, double, and triple bond-order contributions. The bond order is updated at every iteration, which allows ReaxFF to describe the bond formation and bond breaking. Nonbonded interactions, such as van der Waals and Coulomb, are calculated between every pair of atoms, and they are independent from the bonded interactions. Atomic charges are calculated using a geometry-dependent charge calculation scheme, electronegative equalization method (EEM).[21] The ReaxFF method calculates the energy of each atom which governs the dynamics of the system using the following equation

$$E_{system} = E_{bond} + E_{over} + E_{under} + E_{lp} + E_{val} + E_{tor} + E_{vdWaals} + E_{Coulomb} \quad (1)$$

In the above equation, E_{bond} (bond energy), E_{over} (over-coordination penalty energy), E_{under} (undercoordination penalty energy), E_{lp} (lone pair energy), E_{val} (valence angle energy), and E_{tor} (torsion angle energy) are bond-order-dependent terms. $E_{vdWaals}$ (van der Waals energy) and $E_{Coulomb}$ (Coulomb energy) are nonbonded terms. A more detailed description can be found in previous ReaxFF-related papers.[18,19] Recent reviews of the ReaxFF method, and its applications, are given in Senftle et al.[22]

2.2. Reparameterization of the ReaxFF Force Field. The parameters of a ReaxFF force field are typically trained against quantum mechanical (QM) and/or experimental data.[22] The force field parameters can be optimized to reproduce geometries, partial charges, and different types of energies such as reaction energies, reaction barriers, adsorption energies, energies of formation, etc. These QM or experimental data are referred to as the training set data. Each set of training set data is given a weightage based on the importance of the data, and the parameters are optimized until the desired level of accuracy is achieved. The accuracy of the fitting is defined using an error function

$$\text{error}_i = \left(\frac{X_{i,t} - X_{i,ReaxFF}}{\sigma_i} \right)^2$$

where $X_{i,t}$ and $X_{i,ReaxFF}$ are the target quantum mechanical/experimental and ReaxFF values of the ith entry of the training set and σ_i is the inverse weight that determines how accurately the data needs to be fitted with the QM/experimental data. The summation of all errors in the training set provides the overall error, which is one of the measures of the quality of the force field. The parameter optimization is performed using a successive one-parameter search optimization technique.[23] The parameters that require refitting are listed in a "params" file. The params file also lists the interval within which the parameters are allowed to vary. During the four-step optimization process for each parameter, ReaxFF finds an optimized value of that parameter and visits the next parameter in the params file. More details about the training are reported in the later section.

2.3. ReaxFF MD Simulations. The ReaxFF parameter set developed in this work is used to simulate the formation of BNNS using reactive classical MD simulations. Overall, the simulations are performed using the following methodology: first, all of the molecular structures that are part of the initial

https://doi.org/10.1021/acs.jpca.1c09648
J. Phys. Chem. A 2022, 126, 568−582

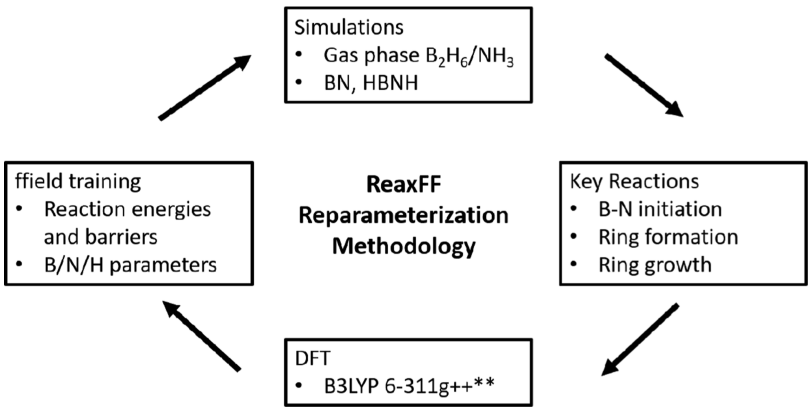

Figure 1. Summary of the ReaxFF force field reparameterization methodology.

simulation configuration are energy minimized. These optimized structures are used to randomly populate a periodic simulation box such that the appropriate density is achieved. All of the configurations presented in this work have a density of 0.02 kg/dm^3 unless mentioned otherwise. This simulation system is then energy minimized at 0 K and equilibrated at a temperature lower than the simulation temperature such that no reactive events are taking place before the final simulation run. The final simulations are performed at the desired temperature using the ADF software suite[24] with the NVT ensemble. The temperature is controlled through the Berendsen thermostat[25] with a temperature damping constant of 100 fs. Following our work with hydrocarbon fuels at higher temperatures,[26,27] the simulations are performed using a time step of 0.1 fs. We identify all reactions that occur during the NVT-MD simulations using an in-house reaction analysis code. When species with different chemical formulae are identified, the in-house code considers that a reaction event has occurred.

2.4. QM Simulations. Density functional theory (DFT) calculations are performed for all of the molecules to calculate bond dissociation energy (BDE) using the Jaguar software package.[28] All geometries are calculated using a hybrid method employing Becke's three-parameters approach, B3LYP,[29] and the 6-311G**++ basis sets.[30]

3. RESULTS AND DISCUSSION

3.1. ReaxFF Force Field Parameter Training. One of the primary aims of this work is to develop a force field capable of describing the BNNS gas-phase synthesis process using B/N/H-related precursors. For this purpose, we started the force field reparameterization based on the Weismiller force field[31] developed for ammonia borane dehydrogenation and combustion. A strategy similar to the one described in Xuan et al.[32] is used here, as shown in Figure 1. First, the Weismiller force field[31] was used to simulate a number of configurations with different B/N/H precursors. These configurations included B_2H_6/NH_3, BN, and HBNH systems. The atomic trajectories from these simulations were analyzed using an in-house code to identify key reaction pathways. Then, DFT calculations were performed for these pathways to calculate the reaction energies as well as barriers. This data was then used to train the force field parameters. This feedback cycle was repeated multiple times until the force field-based reaction energy and barrier predictions were reasonably accurate compared to the DFT data. The advantage of starting with the Weismiller force field[31] is that it was capable of modeling dehydrogenation reactions related to B−N−H species such as ammonia borane.

One of the reasons for the lack of understanding of the growth mechanisms for BNNS is the relative complexity of the B/N/H chemistry. However, we can draw help from the similar, but more comprehensively studied, C/H chemistry. Due to the interest in fossil fuels, soot formation, and more recently graphene, the C/H chemistry has been studied extensively over the last few decades. The first step in understanding the soot formation chemistry is to understand the reaction kinetics of small hydrocarbons. Similarly, along with understanding the ring formation or BNNS formation with precursors like HBNH, it is also important for the force field to be able to correctly describe the B/N gas-phase chemistry, which leads to the formation of these species. Additionally, B_2H_6/NH_3 itself has also been used as precursors in the CVD synthesis of 2D-hBN.[3] Hence, we started our feedback loop reparameterization as displayed in Figure 1 with the B_2H_6/NH_3 configuration. This reparameterization resulted in the training of three types of reactions, which are shown in Table 1.

A more detailed discussion of these reactions is presented in the later sections. Briefly, the precursors first form products such as BH_3 or NH_2. A number of different reactions contribute to these products. For example, BH_3 is produced

Table 1. Comparison of the Reaction Energies of Key Reactions for B_2H_6/NH_3 Precursors between DFT and Reparametrized ReaxFF Force Field

		reaction energy (kcal/mol)	
reaction	class	DFT	ReaxFF
$B_2H_6 > 2BH_3$	*initial*	40.0	39.3
$B_2H_6 > B_2H_4 + H_2$		41.8	37.1
$BH_3 + B_2H_4 > B_3H_7$		−33.8	−33.4
$NH_3 + H > NH_2 + H_2$		−0.9	−3.7
$BH_3 + B_2H_3 > B_3H_6$		−34	−21.3
$NH_2 + BH_3 > H_3BNH_2$	*addition*	−46.9	−50.5
$NH_3 + BH_2 > H_2BNH_3$		−38.1	−42.4
$BH_3 + NH_3 > H_3BNH_3$		−34.2	−28.6
$H_3BNH_3 > H_2BNH_2 + H_2$	*dehydrogenation*	−5.1	−9.2
$H_2BNH_2 > HBNH + H_2$		29.5	36.4
$HBNH > BN + H_2$		132.8	114.5
$HBNH > HBN + 0.5\ H_2$		78.3	57.1
$HBNH > BNH + 0.5\ H_2$		62.9	48.1

https://doi.org/10.1021/acs.jpca.1c09648
J. Phys. Chem. A 2022, 126, 568−582

through the unimolecular decomposition of B_2H_6, while NH_2 typically forms due to extraction of a H atom from NH_3 by another radical. These products then combine to form B/N/H species, which then undergo dehydrogenation to form species that are the key to the formation of six-membered rings. Please note that the Weismiller force field[31] already predicted the reaction energies for dehydrogenation reactions with reasonable accuracy as these reactions were also a part of the force field training for that force field.

After a few iterations of the force field training process, driven by these B_2H_6/NH_3 configurations, we obtained a force field capable of predicting the reaction energetics of these reactions with reasonable accuracy, as shown in Table 1. Subsequently, the simulations of HBNH and borazine configurations were added to the feedback process depicted in Figure 1. Here, to once again connect to hydrocarbon chemistry, HBNH and borazine can be considered equivalent to acetylene and benzene, respectively. As such, they are key to the formation of the first ring and the growth of the ring structures. Table 2 shows the comparison of the key reaction energetics for the reactions involving these two precursors, including the addition of dehydrogenated B−N−H products and cyclization reactions. Along with these key reactions, we have also added the formation energies of flat as well as closed BN nanostructures similar to the ones described by Krstic et al.[15] These are important to correctly capture the final shapes of nanostructures.

Table 2. Comparison of the Reaction Energies of Key Reactions Related to Ring Formation

	reaction energies (kcal/mol)	
reaction	DFT	ReaxFF
HBN + BNH > $B_2N_2H_2$	−155.9	−136.3
B_2N_2H + BNH > $B_3N_3H_2$	−151.4	−148.4
B_2N_2H + HBN > $B_3N_3H_2$	−159.8	−145.4
B_3N_3 cyclization	−101.4	−92.7
3 HBNH > $B_3N_3H_6$	−156	−165.7

Figure 2 shows overall improvements in the force field after reparameterization with the additional data. The new force field retains or improves the agreement of the training data related to the B−N−H from the Weismiller force field.[31] The mean energy difference with the DFT data reduces from 35 to 17 kcal/mol during reparameterization. The training of force field parameters often involves a trade-off between prioritizing the accuracy of certain reaction over others. For example, the reactions presented in Table 1 were considered highly important and, as such, were given a higher weight in the training, and for that reason provide a better match than the mean energy difference value.

3.2. B/N/H Gas-Phase Chemistry. As explained previously, understanding the B/N gas-phase chemistry is the first step in the investigation of BNNS formation. In this subsection, we will discuss the results obtained from a set B_2H_6/NH_3 simulations at 2500 K with a corresponding initial real gas pressure of 180 bar. The starting configuration consists of 1000 NH_3 and 40 B_2H_6 molecules. The higher percentage of NH_3 is chosen here as it is necessary to form B−N species similar to the experiments.[5] Diborane is much more reactive than ammonia and readily decomposes to either BH_3 or B_2H_4 species, as shown in Table 1. Figure 3 shows the number densities of important species with the highest concentrations. We observe that both B_2H_6 and BH_3 get consumed much faster than ammonia, as shown in Figure 3b. These species can react with each other to form B−B clusters. Hence, a higher concentration of B_2H_6 results in boron clusters mainly comprised of B−B bonds. This is similar to the observation made by Sun et al.[33] in their computational study of diborane pyrolysis. Hence, it is important to have a high NH_3 concentration to form species containing BN bonds. NH_3 can readily react with BH_3 to form amino borane. However, we also observed hydrogen abstraction from ammonia leading to NH_2, which could also lead to the formation of B−N species.

The major products observed in our simulations include H_2 (see Figure 3a) and a set of B−N species such as BNH_2, BN_3H_6, and BN_2H_3, as shown in Figure 3c. Figure 4 shows the structure of the key early species along with some of the largest species formed toward the end of the 1 ns simulation time. The simulation successfully forms a set of BN species along with the BN ring containing species at the end of 1 ns simulation. These products follow the B−N gas-phase chemistry outlined in the earlier section; the reactants or their immediate products such as BH_3, BH_2, NH_3, or NH_2 combine to form the BNH_x species. These species subsequently undergo dehydrogenation to form products such as HBNH or BN_2H_3. Thereafter, these products can combine to form larger species, including ring structures, as shown in Figure 4. These observations validate the capability of the force field to model the B−N gas-phase chemistry up to the early ring formation stage. Additionally,

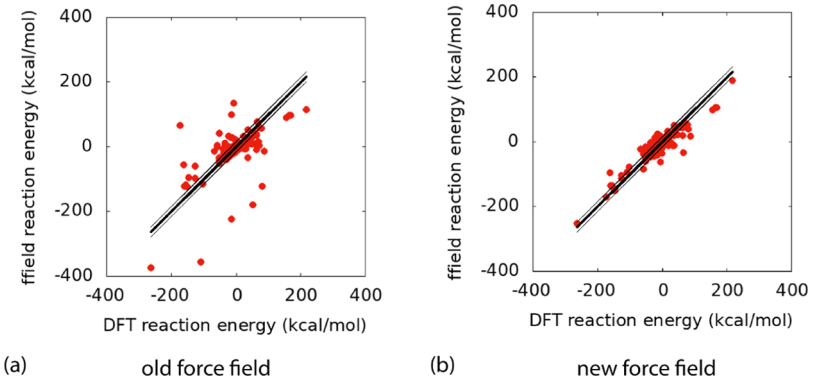

Figure 2. Overall force field training errors for the additional DFT data. The figure on the left is for the old force field, and the one on the right is for the new force field. The bold black line represents the ideal match with the DFT data, while the thin black lines represent a 15 kcal/mol variation with the DFT training data.

https://doi.org/10.1021/acs.jpca.1c09648
J. Phys. Chem. A 2022, 126, 568−582

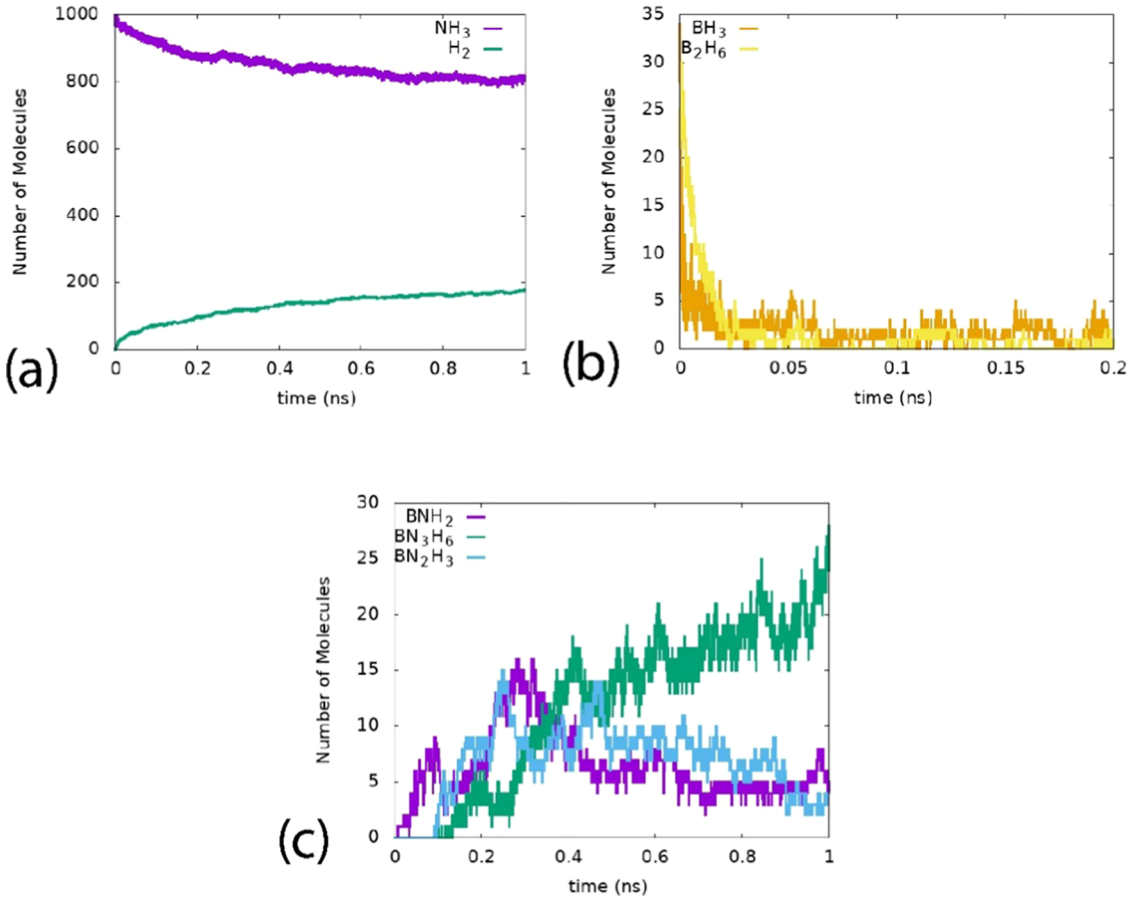

Figure 3. Species number density for the B_2H_6/NH_3 simulation major species.

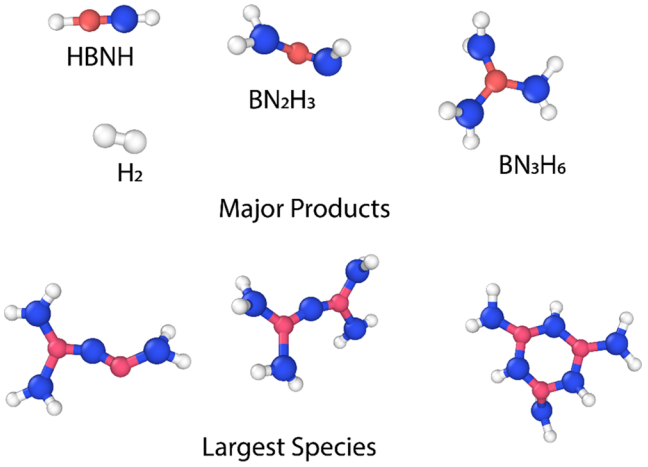

Figure 4. Major products and the largest species at the end of the simulations.

B−N species along with a ring species are formed in a nanosecond time scale. Although ReaxFF simulations employ relatively high pressure to accelerate the simulations, the higher pressure does not affect the type of reactions that are occurring.[34] Hence, we can expect similar reactivity in micro- or millisecond scale when using lower pressures of the order of few bars or below. This could mean that when B_2H_6/NH_3 are used as precursors for the CVD synthesis of 2D-hBN, significant reactions could happen in the gas phase affecting the growth of the hBN. As such, understanding the gas-phase chemistry is important to understand the formation of 2D-hBN on a substrate surface during the CVD synthesis. Longer and larger simulations will be required to observe the formation of large multiple ring species or BNNS, which is discussed in the next sections—starting from BN precursors.

3.3. BNNS Formation with HBNH and BN Precursors.

In this section, we discuss the formation of BNNS with HBNH and BN precursors. These precursors can potentially be used in gas-phase synthesis methods.[4−6,8,9] Additionally, HBNH is an important product of the B_2H_6/NH_3 configuration, which is used for the CVD synthesis of 2D-hBN.

3.3.1. HBNH Precursors. Figure 5 shows the number of six-membered rings observed during HBNH simulations. These simulations are performed with 700 HBNH molecules at 2000 K at different stages along with the simulation with a corresponding initial real gas pressure of 73 bar. A recent experimental study by Bansal et al.[35] employs similar temperatures to synthesize hBN on a sapphire substrate with B_2H_6/NH_3 as precursors. Their work suggests that the precursor species might undergo chemical reactions before reaching the substrate surface. The ReaxFF parameters developed in this work can be used to identify this chemical reactivity similar to some of the previous work by our research group.[32] As HBNH is an important product in this process, as indicated by simulations discussed earlier, the following results might help us explain the gas-phase reactivity for the abovementioned synthesis process. The overall simulation can be divided into three stages. In the first stage of the simulation, the precursor species react with each other to form the initial ring structures till ∼0.6 ns. We predominantly

https://doi.org/10.1021/acs.jpca.1c09648
J. Phys. Chem. A 2022, 126, 568−582

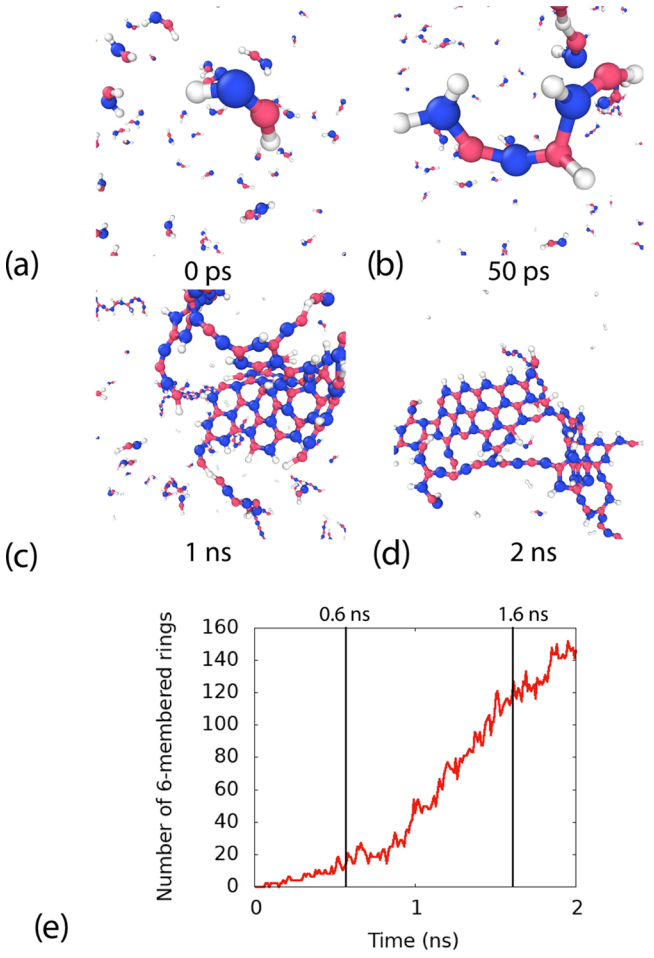

Figure 5. Representative simulations snapshots at (a) 0 ns, (b) 50 ps, (c) 1 ns, (d) 2 ns, and (e) the number of six-membered rings in the simulation as a function of time for HBNH precursor simulations at 2000 K.

observe single-ring structures until this point. The HBNH species first form small chains comprising of multiple BN bonds typically up to $B_4N_4H_x$. These 1D structures then grow, branch, and eventually form six-membered rings. Most of the initial six-membered ring species have a small side chain attached to them, indicating that they are formed through pathways involving species larger than $B_3N_3H_x$. This is followed by the second phase from ∼0.6 to 1.6 ns in which these species grow to form multiple ring species. The third stage can be considered from ∼1.6 to 2 ns where the multiple ring species combine together to form larger species, as shown in Figure 5d. These regimes can overlap with each other. For example, the large molecules can still increase their number of rings even after combining with other large species. This growth pattern is also reflected in Figure 5e showing the number of six-membered rings as a function of time. We see initial slow ring formation—until around t = 0.6 ns—followed by a steady, fast ring formation stage that lasts until t = 1.6 ns, after which ring growth slows down slightly due to the lack of the precursor and subsequently formed $B_xN_yH_z$ species of low molecular weight.

Figure 6 shows a typical growth pathway for one of the larger species at the end of the simulation. As described earlier, in the first stage, HBNH undergoes partial dehydrogenation followed by recombination to form larger $B_xN_xH_y$ species.

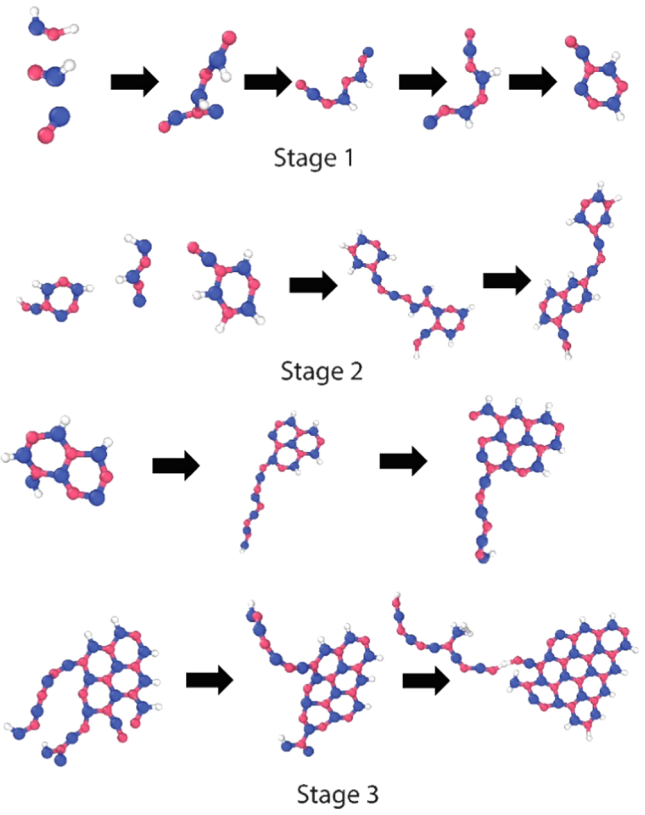

Figure 6. Typical BNNS formation stages for the HBNH precursor.

Please note that this is not the only pathway through which the large species formation takes place—this is just one representative pathway that we show by retracing the formation of one of the largest species formed during the simulation. Analyzing Figure 6, it is interesting to note that in the second stage, most of the growth takes place through combination and rearrangement of relatively large species rather than smaller ones, like HBN, BNH, or HBNH precursors, added to the larger species. Another major route for the ring growth is the rearrangement of the attached polymer chains to form additional rings, as shown in the Stage 3 snapshots. Also note that all rings are at the edges terminated by H atoms. This is essential to form flat BNNS rather than closed BNNS. This indicates that H atoms play an important role in forming flat BNNS as discussed in the next sections.

3.3.2. BN Precursors. Figure 7 shows the number of six-membered rings formed from the BN precursor at 2000 K with corresponding initial gas pressure of 142 bar with 729 precursor molecules. Here, the BN precursor can easily polymerize to form long BN chains with infrequent interconnects, as seen in Figure 7c. It is challenging to track the reactions happening in the case of these simulations since very large interconnects of BN polymers are formed due to branching before the formation of the first ring. Here, the ring formation mechanism is different from that with the HBNH precursor.

Based on the observations from the simulation trajectories of large species, the formation of BNNS can be divided into three stages. In the first stage, which lasts up to ∼0.1 ps, BN dimers add up to form small BN polymers. These polymers can combine to form amorphous structures similar to those shown in Figure 7c. The next stage involves these structures further combining to form even larger structures. This process of

https://doi.org/10.1021/acs.jpca.1c09648
J. Phys. Chem. A 2022, 126, 568−582

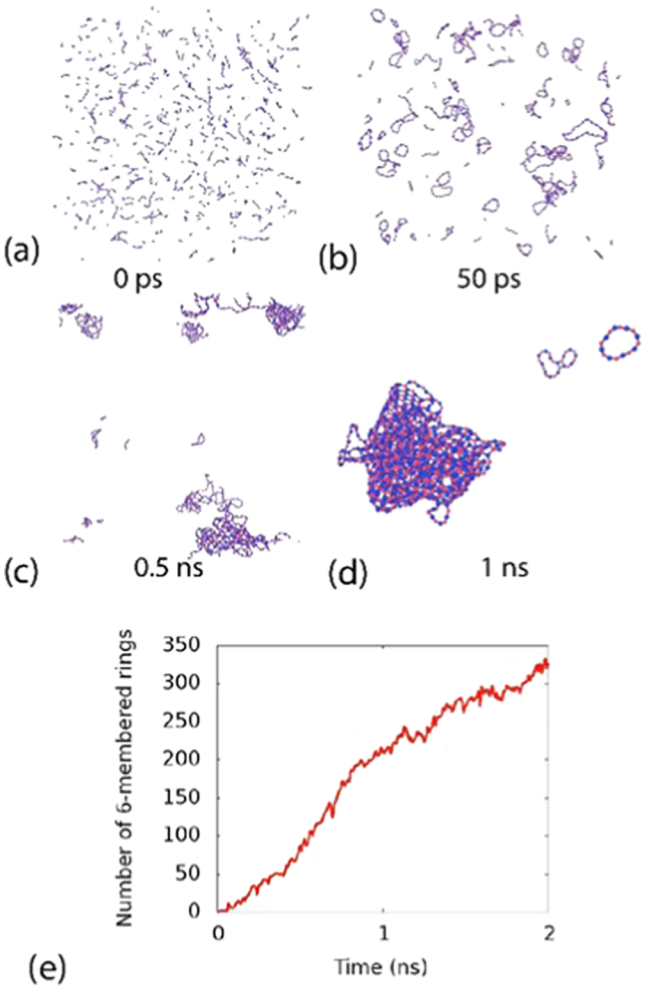

Figure 7. Representative simulations snapshots at (a) 0 ns, (b) 50 ps, (c) 0.5 ns, (d) 1 ns, and (e) the number of six-membered rings in the simulation as a function of time for BN precursor simulations at 2000 K.

formation of large nanostructures at the expense of smaller ones is known as Oswald ripening.[36,37] These larger structures have both polymeric and 2D-hBN characteristics (see Figure 8 stage 2). The ring formation and growth is not as distinct as in the case of the HBNH precursor. The ring formation starts at BN interconnects in the polymeric structures. The large BN structure keeps rearranging itself to form more and more six-membered rings.

Figure 9 shows a sliced view of the BNNS formed by the BN precursor simulation at 2 ns. As pointed out by Krstic et al.,[15] the BN precursor leads to the formation of closed structures compared to the flat, H-terminated structures with the HBNH precursor. Due to the absence of ring-terminating H atoms, BN structures do not remain flat. Instead, curved structures are formed ultimately leading to closed structures. The sliced view of the final structure in Figure 9 shows that the final structure can be described as a cocoon-like structure or a single-walled BNNT with closed ends.

3.4. Quality of BNNS. As we have seen in the previous sections, not only do different precursors have different mechanisms leading to BNNS, the types of structures formed are also different. To define the quality of the structures formed in the simulations, we use a quality factor (QF) to assess the larger structures formed during the simulations. The

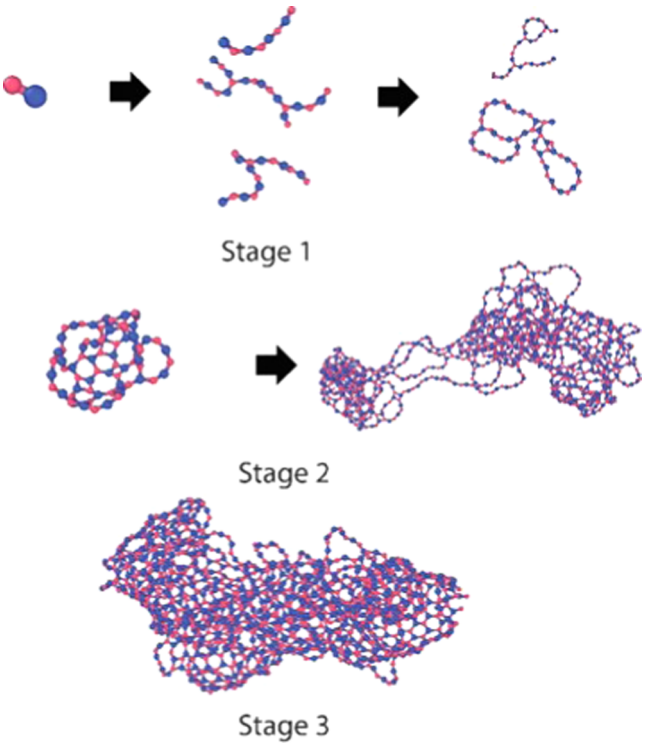

Figure 8. Typical BNNS formation stages for the BN precursor.

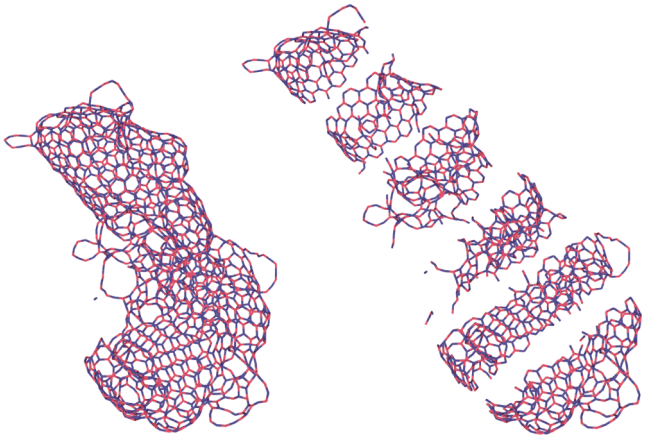

Figure 9. Sliced view of the BNNS formed by the BN precursor at 2 ns of 2000 K simulation. The structure on the left shows the final closed BNNS structures formed by a BN precursor. The structure on the right shows the slices of the same structure obtained by dividing the structure using planes perpendicular to the longer dimension of the structure.

work of Krstic et al.[15] also defined a similar quality factor. A brief description of the quality factor can be found in the Supporting Material. Briefly, it is a factor comparing the number of six-membered rings in a given structure to the optimal number of six-membered rings that can be formed with a given number of particles. For n number of particles, the optimal number of six-membered rings formed can be calculated as

$$\text{maximum number of hexagons for } n \text{ particles} = \frac{(n-10)}{3} + 2$$

https://doi.org/10.1021/acs.jpca.1c09648
J. Phys. Chem. A 2022, 126, 568−582

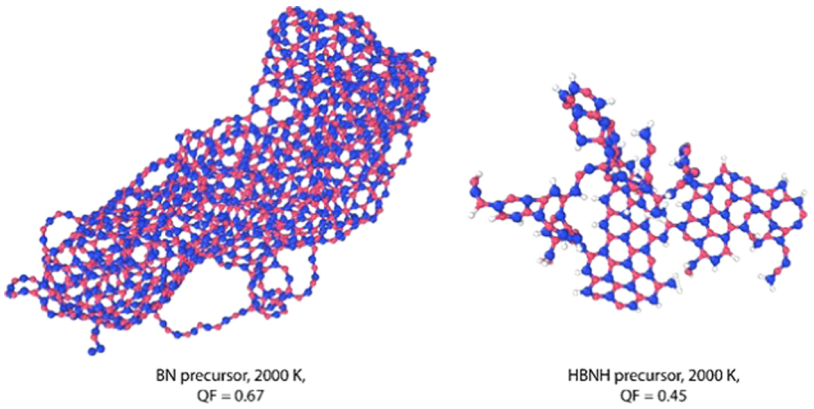

Figure 10. Quality of the largest structure obtained from BN and HBNH precursor simulations, respectively.

Therefore, the quality factor can be defined using a simple expression

$$\mathrm{QF} = \frac{\text{actual number of hexagons}}{\mathrm{NX}}$$

Any defect in a BNNS ends up reducing the number of six-membered rings in the structure. Hence, a larger quality factor represents better structure. Figure 10 shows two large final structures formed in the HBNH and BN precursor simulations, respectively.

Similarly, the QF can also be calculated for an entire simulation configuration by averaging the QF for each species in a given frame. This allows us to calculate the overall quality as well as ring growth of the BNNS as the simulation progresses.

$$\mathrm{OQF} = \sum_{\text{all species}} \text{mass fraction}^{*}\mathrm{QF}$$

Figure 11 compares the overall quality factor (OQF) for BN and HBNH precursor simulations as a function of time at 2000 K. It is clear from this comparison that the BN precursor forms better structures. Please note that although the overall quality of the BNNS formed by the BN precursor is higher, it will always lead to the formation of a closed or curved structure. Obtaining flat 2D-hBN structures would require H-containing precursors like HBNH. The final structure in the case of the HBNH precursor is made of a set of smaller hydrogen-terminated BNNS, as seen in Figure 11. The QF and OQF give a straightforward numerical criterion to assess the quality of a BNNS. Hence, we obtain conclusions similar to those obtained by the QCMD.[15]

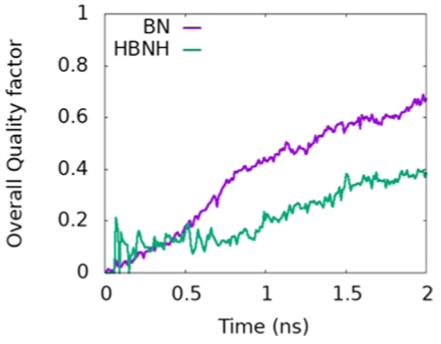

Figure 11. Overall quality factor as a function of time for BN and HBNH precursor simulations as a function of time at 2000 K.

3.5. Effect of Temperature and Pressure. Operating conditions also play a major role in BNNS formation as well as the quality of BNNS structures. To evaluate the role of these conditions, we performed precursor simulations at three different temperatures and densities to understand the effect of temperature and pressure on BNNS formation. In this section, we discuss the main observations from these simulations. Figure 12 shows the number of six-membered rings as a function of time for three different temperatures for the BN precursor. The simulation at 2500 K yields very few six-membered rings, while the ring formation is better at lower temperatures. As explained previously in the section discussing BN precursor simulations, the BNs quickly form rather large polymers. Hence, it is difficult to single out a specific reaction or group of reactions responsible for this behavior.

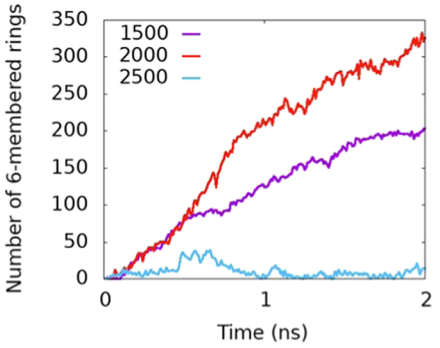

Figure 12. Number of six-membered rings as a function of time at 1500, 2000, and 2500 K for the BN precursor.

To investigate this behavior further, we calculated the Gibbs free energies for a large polymer and for a 2D-hBN structure with the same number of B and N atoms. Figure 13 shows the difference in the Gibbs free energies between a polymeric and a 2D-hBN structure with the same number of B and N atoms. As the temperature increases, the 2D-hBN structure becomes increasingly less favorable. This can be explained using the entropies for these structures shown in Table 3. Due to its highly structured nature, 2D-hBN has lower entropy compared to the polymeric BN. This difference keeps increasing with temperature. Hence, the Gibbs free-energy slope reduces with increasing temperature. This underlines the importance of temperature in the BNNS formation. Krstic et al.[15] also make

https://doi.org/10.1021/acs.jpca.1c09648
J. Phys. Chem. A 2022, 126, 568−582

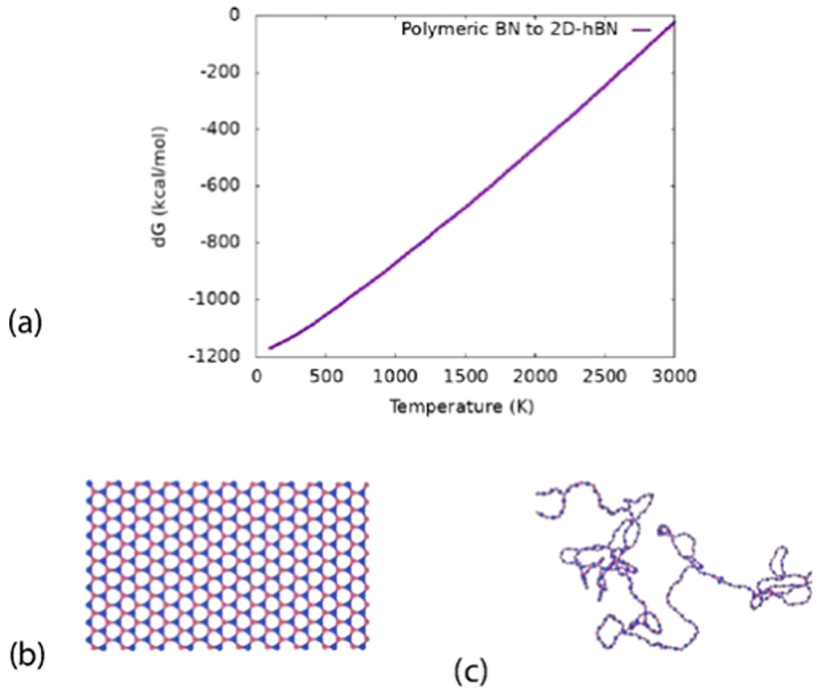

Figure 13. (a) Gibbs free-energy change as a function of temperature for the structural change to (b) 2D-hBN from (c) polymeric BN.

Table 3. Comparison of Entropy at Different Temperatures between Polymeric BN and 2D-hBN

	entropy (cal/mol-K)	
temperature (K)	2D-hBN	polymeric BN
500	1156.66	1501.26
1000	2101.42	2483.06
1500	2768.79	3174.45
2000	3271.45	3697.16
2500	3671.54	4114.24
3000	4002.83	4460.12

similar observations in the case of BN precursors. Very high temperatures are undesirable for a BN precursor, which would lead to the formation of B only species. Hence, temperature needs to be optimized properly to attain optimal yield during the synthesis process.

Figure 14 shows the number of six-membered rings for the HBNH precursor. Here the ring formation process is not limited by the rearrangement of large polymer species. Hence, we observe significant six-membered ring formation at high temperatures due to the involvement of H atoms. An interesting note here is that similar to the BN precursor, the lower temperature (1500 K) mainly helps in the initial part, where it results in a higher rate of six-membered ring formations. If the simulations are run long enough, then we see that the higher temperature catches up in terms of the number of six-membered rings formed.

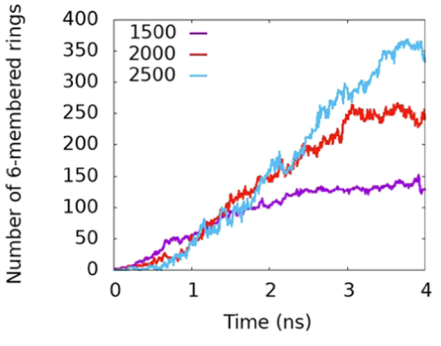

Figure 14. Number of six-membered rings as a function of time at 1500, 2000, and 2500 K for the HBNH precursor.

Figure 15 shows the effect of change of density on the ring formation process. Increasing the pressure of a precursor typically accelerates the reactions and hence higher pressure leads to a higher rate of six-membered ring formation. This agrees well with the experimental studies which suggest that using higher pressure aids the synthesis of BNNTs in the gas phase.[9,10]

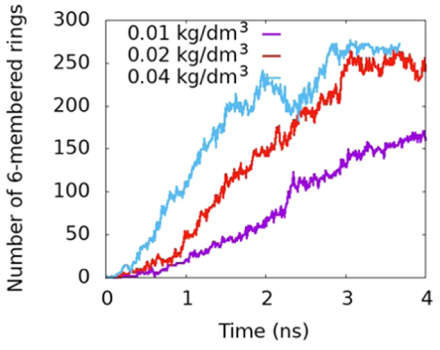

Figure 15. Number of six-membered rings as a function of time at 0.01, 0.02, and 0.04 kg/dm^3 for the HBNH precursor.

Figure 16 shows the quality factor as a function of time at different temperatures and pressures with HBNH as a precursor. The lower temperature simulation forms higher-quality structures initially. However, the number of six-membered rings, as well as the quality of structures, becomes similar at around 2 ns for all of the temperatures. However, if we continue the simulations longer, higher-temperature

https://doi.org/10.1021/acs.jpca.1c09648
J. Phys. Chem. A 2022, 126, 568−582

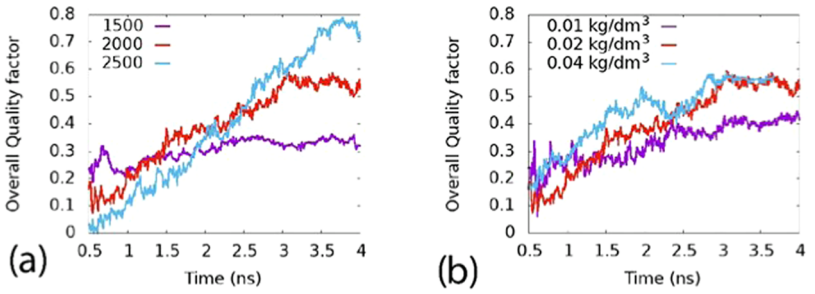

Figure 16. Effect of (a) temperature and (b) density on the quality of the BNNS for the HBNH precursor. The temperature simulations are performed at the density of 0.02 kg/dm^3, and varying density simulations are performed at 2000 K.

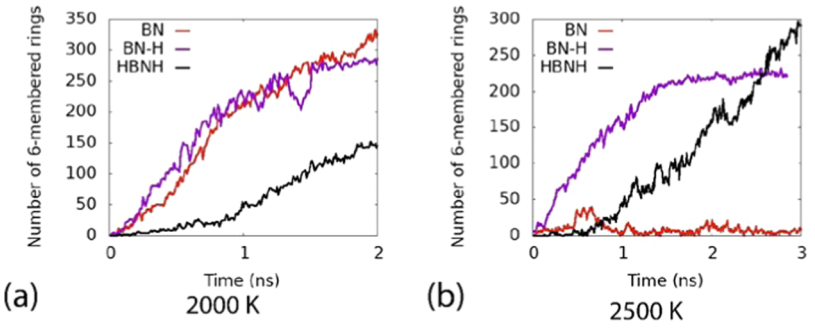

Figure 17. Effect of adding H to BN precursor simulations. The images show the number of six-membered rings as a function of time for BN, BN−H, and HBNH precursor simulations at (a) 2000 and (b) 2500 K.

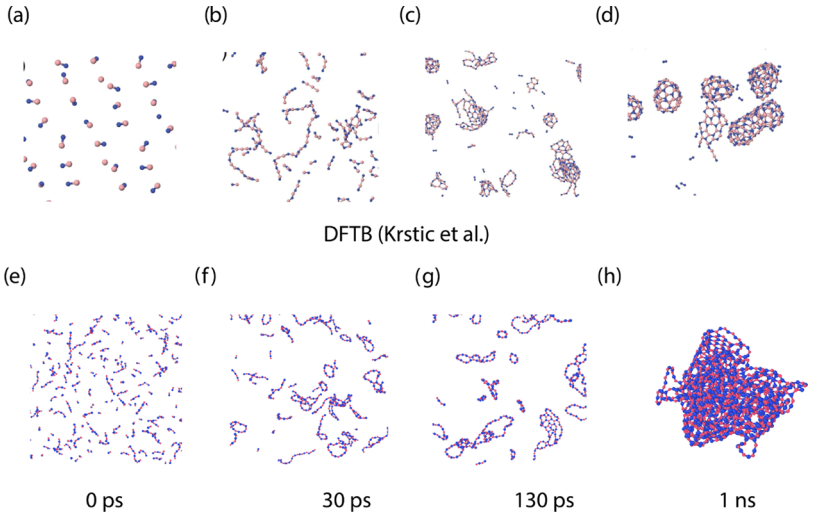

Figure 18. Comparison between (a−d) DFTB (Reproduced from ref 15 with permission from the Royal Society of Chemistry.) and (e−h) ReaxFF trajectories for the BN precursor at 2000 K.

simulations lead to much better quality structures. Please note that we are showing QF only after 0.5 ns to ignore initial fluctuations. A lower pressure leads to lower initial OQF values, which increase during a simulation, getting closer to the higher density OQF values after t = 3 ns. In summary, if we compare BNNS with a similar number of six-membered rings obtained at different temperatures or pressures, the quality of the BNNS is likely to be similar as well. The BNNS quality is mainly driven by the precursor choice.

3.6. Effect of Additives on BNNS Formation. Another important variable in the BNNS formation, apart from the precursor, temperature and pressure, are additives. Additives such as H_2 can be intentionally added or are a part of the synthesis procedure as, for example, a carrier gas. As a representative case, Figure 17 shows the effect of the addition of H to a BN precursor simulation. One hundred hydrogen atoms are added to the BN simulation configuration while keeping the density constant. HBNH precursor data is also shown for comparison. BN and HBNH simulations are representative of two extreme cases in terms of hydrogen presence with the BN−H simulations describing an intermediate scenario. The number of six-membered rings formed is similar for BN and BN−H cases at 2000 K. However, at 2500 K, the addition of H greatly improves the number of six-membered rings. At this higher temperature of 2500 K, the HBNH precursor overtakes both BN and BN−H precursors in terms of the number of six-membered rings formed. This observation clearly indicates that the addition of H would aid

https://doi.org/10.1021/acs.jpca.1c09648
J. Phys. Chem. A 2022, 126, 568−582

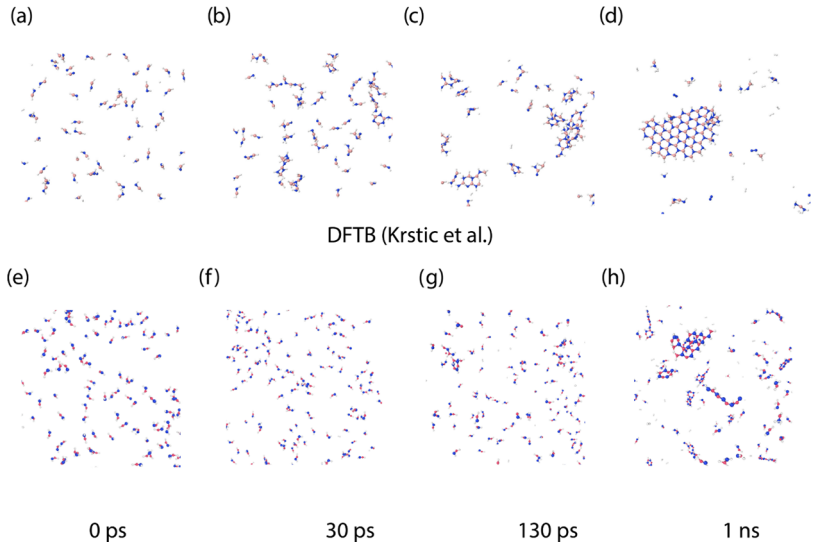

Figure 19. Comparison between (a–d) DFTB[15] and (e–h) ReaxFF trajectories for the HBNH precursor at 2000 K. The orange, blue, and white spheres represent B, N, and H atoms, respectively.

Table 4. Comparison between DFTB, ReaxFF, and DFT Reaction Energies for the Key Reactions in HBNH Precursor Simulations[a]

Reaction	Reaction Energy (kcal/mol)		
	DFT	DFTB	ReaxFF
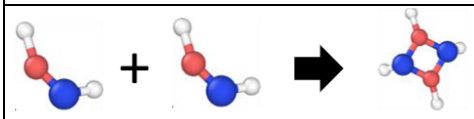	-68.9	-63.3	-59.8
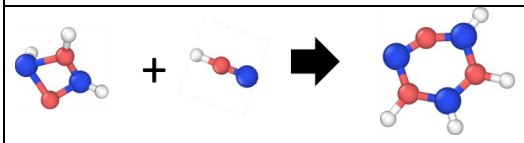	-146.1	-202.3	-148.5
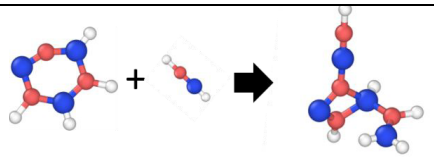	-9.2	-21.85	-3.7
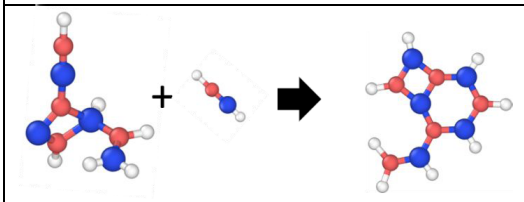	-127	-117.6	-111.0

[a]The orange, blue, and white spheres represent B, N, and H atoms, respectively.

the BNNS formation at higher temperatures. However, high temperatures (like 4000 K[15]) would lead to dominant formation of boron clusters. A similar observation was made experimentally by Kim et al.[6] as well. Briefly, in the experimental work of Kim et al.,[6] B-containing feedstocks are vaporized at high temperatures above 3000 K to form nanosized B droplets. BNNT grows continuously from those B droplets by incorporation of N-containing species such as N_2. Due to the relatively inert nature of N_2, this process is slow and results in the low yield of BNNT. However, the synthesis of BNNT is greatly assisted by the presence of H_2. The addition of H_2 leads to the formation of B/N/H species, which leads to the faster synthesis of BNNT with better yield. The formation of BNNT takes place at a lower temperature of

https://doi.org/10.1021/acs.jpca.1c09648
J. Phys. Chem. A 2022, 126, 568–582

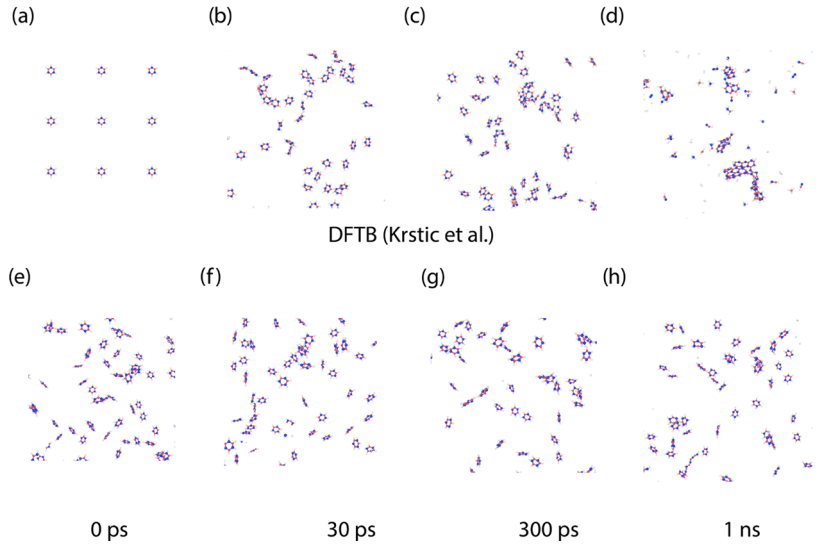

Figure 20. Comparison between (a−d) DFTB (Reproduced from ref 15 with permission from the Royal Society of Chemistry.) and (e−h) ReaxFF trajectories for the borazine precursor at 2000 K. The orange, blue, and white spheres represent B, N, and H atoms, respectively.

around 2000 K. The simulations presented here indicate similar behavior.

3.7. Comparison with Existing Work. Krstic et al.[15] used QCMD based on DC−DFTB-K[38] to simulate the synthesis of BNNS in a hot, high-pressure gas volume. They studied the formation of BNNS using different precursors, including BN, BN−H, HBNH, and $B_3N_3H_6$. It is one of the few modeling studies trying to understand the growth mechanism of BNNS at high temperatures. More details about DFTB simulations can be found in the original manuscript.[15] Here, we compare some of the results obtained using the ReaxFF force field developed in the current work with the work of Krstic et al.[15]

Figure 18 compares simulation snapshots at different stages during the BN precursor simulation. Both the simulations follow similar trends initially, where the BN precursor combines up to form B_xN_x chains. Both the simulations start forming six-membered ring structures at 130 ps. There are two key differences between DFTB and ReaxFF for these simulations. First, at the end of 1 ns simulation time, ReaxFF simulations form a large single structure, whereas DFTB simulations form smaller nanocages. However, even with ReaxFF simulations, the formation of nanocage-like structures is the precursor step to the formation of larger structures. Hence, in this case, ReaxFF simulations are faster than DFTB. The second difference is based on temperature dependence. The DFTB simulations form a significant number of rings at 2500 K. However, ReaxFF simulations indicate that at 2300 K, BNNS formation with the BN precursor hits a critical point. As indicated by the Gibbs free-energy analysis, the free-energy difference between an hBN-type structure and a polymeric structure reduces with increasing temperature. Hence, at 2500 K, the BN precursor forms polymeric structures instead of hBN-type structures.

Figure 19 shows a similar comparison for the HBNH precursor. In these simulations, both ReaxFF and DFTB lead to flat hBN structures. As pointed out earlier, the H atoms at the edges do not allow the formation of closed structures similar to the BN precursor. Here, ReaxFF is relatively slower compared to DFTB in forming six-membered rings. For example, ReaxFF simulations take 1 ns to form structures of a similar size to those observed in the DFTB simulation screenshot at 130 ps. The ReaxFF simulations eventually lead to similar structures, as shown in the 1 ns screenshot of the DFTB simulations and 2 ns screenshot of the ReaxFF simulations (see Figures 19d and 5d, respectively).

Again, to investigate this, we compare the reaction energies of key reactions extracted using DFTB simulation trajectories between ReaxFF, DFTB, and DFT, as shown in Table 4. Here, DFTB simulations are performed using ADF software suite using the MATSCI package. These are some of the frequent reactions responsible for the first ring formation and ring growth obtained by retracing common species along the simulation trajectories. Although, for two of these reactions, both ReaxFF and DFTB show comparable results to that of DFT, DFTB energetically favors the two intermediate steps. This could potentially speed up the six-membered ring formation in DFTB simulations leading to early ring formation and faster ring growth.

Again, a similar comparison is performed for borazine. This comparison also shows similar trends as that of HBNH simulations. ReaxFF simulations (see Figure 20e−h) are much slower compared to the DFTB simulations (see Figure 20a−d) in forming six-membered ring clusters. The ReaxFF simulations do not form flat hBN structures, as shown by DFTB simulation snapshots within the same timeframe of 1 ns. However, upon continuing ReaxFF simulations further up to 4 ns leads to the formation of flat hBN structures similar to the ones formed by the DFTB simulation at the end of 1 ns simulation time (see Supporting Material, Figure S2). Again, to assess this difference, we compare the energetics of some key reactions responsible for the ring growth process in the case of borazine as a precursor in Table 5.

Similar to the case of HBNH, we analyzed DFTB and ReaxFF trajectories to identify important initial reactions. In this case (borazine), dimerization of borazine was the most dominant reaction apart from the dehydrogenation of borazine. Hence, we compare the reaction energies for these reactions. In this comparison, ReaxFF has lower reaction energy for dehydrogenation reactions. However, it takes additional reaction steps for the products of dehydrogenation such as $B_3N_3H_5$ to form multiple six-membered ring structures. Then, the key reaction for ring growth from DFTB simulations

https://doi.org/10.1021/acs.jpca.1c09648
J. Phys. Chem. A 2022, 126, 568−582

Table 5. Comparison of Reaction Energies between ReaxFF, DFT, and DFTB

reaction	reaction energy (kcal/mol) DFTB	ReaxFF	DFT
$B_3N_3H_6 \rightarrow B_3N_3H_5 + 0.5\ H_2$ (from B)	89.6	41.1	57.4
$B_3N_3H_6 \rightarrow B_3N_3H_5 + 0.5\ H_2$ (from N)	84.2	33.3	67.7
$B_3N_3H_6 + 0.5\ H_2$ (to B) $\rightarrow B_3N_3H_7$	24.6	28.6	47.5
$B_3N_3H_6 + 0.5\ H_2$ (to N) $\rightarrow B_3N_3H_7$	40.8	36.4	62.7
$2^*B_3N_3H_6 \rightarrow B_6N_6H_{12}$ (dimer)	−20.7	5.6	33.2

is through dimerization of borazine. This reaction is energetically favored in DFTB simulations, whereas it is 33.2 kcal/mol uphill according to DFT simulations. This reaction provides a direct route for multiple ring formation and growth, leading to an explanation for the lower time required by DFTB simulations to form flat BNNS compared to ReaxFF. We note that ReaxFF also underestimates the H-abstraction energy as well as the dimerization energy. Hence, it is likely that both the DFTB and ReaxFF simulations overestimate the formation rate of BNNS with the borazine precursor.

In summary for the BN precursor, ReaxFF and DFTB show similar BNNS formation mechanisms and rates. ReaxFF leads to the formation of a large cocoon-like structure, whereas DFTB simulations form multiple smaller closed structures. In the case of HBNH and borazine, ReaxFF shows lower reactivity compared to DFTB simulations potentially explained by the reaction energetics as described earlier. It is clear from the comparisons that DFTB and ReaxFF both predict similar mechanisms for the formation of BNNS. However, DFTB simulations show significant differences in terms of reaction energetics for some of the key reactions when compared to DFT. This results in DFTB simulations showing BNNS growth in a shorter timeframe compared to that of ReaxFF. ReaxFF shows a fair match with DFT results. We found that none of the methods consistently showed better accuracy than the other when compared to DFT. Hence, the comparison is not adequate to comment on the higher accuracy of one method or the other. Rather, these observations indicate that the DFTB simulations could potentially serve as a guide to the ReaxFF parameter development. The initial training of ReaxFF parameters as discussed in Section 3.1 can be performed with DFTB instead of DFT to reduce computational cost followed by more accurate DFT calculations. Then, orders of magnitude lower computational cost of ReaxFF compared to DFTB and DFT can be exploited to perform larger-scale simulations.

4. CONCLUSIONS

The Weismiller force field[31] was reparametrized to make it suitable for B/N gas-phase chemistry and BNNS formation simulations at elevated temperatures. A feedback loop extracting information on new structures from MD simulations feeding to DFT calculations is used here. This DFT data is then, in turn, added to the ReaxFF training set and used to reparametrize the force field. The force field training involves training for reactions related to the B−N gas-phase chemistry resulting in B−N bond-containing species. It also involves training for ring formation pathways. The resultant force field gives a good reproduction of the DFT data for around 60 reaction energies and barriers.

The updated B/N/H 2021 force field parameters were subsequently used to investigate the B−N gas-phase chemistry and BNNS formation. The gas-phase chemistry was investigated using B_2H_6/NH_3 simulations. The simulations show that HBNH is one of the important products which could potentially lead to BNNS formation when B_2H_6/NH_3 is used as a precursor in the CVD synthesis of 2D-hBN. We also observe the formation of species containing six-membered rings in our simulations. This suggests that the gas-phase chemistry of B_2H_6/NH_3 will play an important role in understanding the CVD synthesis of 2D-hBN.

To investigate the high-temperature synthesis of BNNS, BN, and HBNH are chosen as representative precursor examples. The effect of different operating conditions is also investigated. The simulations show that BN is the best of these two precursors in terms of quality and the size of the BNNS. However, the BNNS are converted to complex polymeric structures at temperatures of 2500 K and higher due to entropic effects. Compared to a BN precursor, HBNH forms relatively small and low-quality BNNS, but it is less affected by temperature. More importantly, the BN precursor leads to the formation of closed structures, whereas the HBNH precursor forms flat H-terminated 2D-hBN structures. Additives like H_2 significantly affect the BNNS formation. In summary, the results show the capability of the force field in predicting the BN gas-phase chemistry and BNNS formation.

The time scales involved in CVD synthesis with B_2H_6/NH_3 precursors will require large time scale MD simulations, which are beyond the scope of this work. However, reaction mechanisms extracted from the higher-temperature MD simulations can potentially be coupled with CFD simulations to simulate the CVD synthesis process, as demonstrated by Xuan and co-workers for 2D-chalcogenide growth.[32] Additional work is also required in understanding the role of substrates, like alumina surfaces, in CVD synthesis. All this work, including longer MD simulations, MD-CFD-coupled simulations, and modeling substrate interactions, will be undertaken as a part of the future work.

■ ASSOCIATED CONTENT

Supporting Information

The Supporting Information is available free of charge at https://pubs.acs.org/doi/10.1021/acs.jpca.1c09648.

Details of calculating quality factor and additional simulation snapshot (PDF)

ReaxFF force field parameters (TXT)

■ AUTHOR INFORMATION

Corresponding Author

Adri C. T. van Duin − *Department of Mechanical Engineering, The Pennsylvania State University, University Park, Pennsylvania 16802, United States;* orcid.org/0000-0002-3478-4945; Email: acv13@psu.edu

Authors

Aditya Lele − *Department of Mechanical Engineering, The Pennsylvania State University, University Park, Pennsylvania 16802, United States;* orcid.org/0000-0002-1558-1560

Predrag Krstic − *Institute for Advanced Computational Science, Stony Brook University, Stony Brook, New York 11794, United States;* orcid.org/0000-0001-8326-2978

Complete contact information is available at: https://pubs.acs.org/10.1021/acs.jpca.1c09648

Notes

The authors declare no competing financial interest.

■ ACKNOWLEDGMENTS

The authors acknowledge funding support from National Science Foundation (NSF) through the Pennsylvania State University 2D Crystal Consortium—Materials Innovation Platform (2DCC-MIP) under NSF cooperative agreements DMR-1539916 and DMR 2039351.

■ REFERENCES

(1) Kubota, Y.; Watanabe, K.; Tsuda, O.; Taniguchi, T. Deep Ultraviolet Light-Emitting Hexagonal Boron Nitride Synthesized at Atmospheric Pressure. *Science* **2007**, *317*, 932−934.
(2) Zhang, K.; Feng, Y.; Wang, F.; Yang, Z.; Wang, J. Two Dimensional Hexagonal Boron Nitride (2D-HBN): Synthesis, Properties and Applications. *J. Mater. Chem. C* **2017**, *5*, 11992−12022.
(3) Wang, H.; Zhao, Y.; Xie, Y.; Ma, X.; Zhang, X. Recent Progress in Synthesis of Two-Dimensional Hexagonal Boron Nitride. *J. Semicond.* **2017**, *38*, No. 031003.
(4) Yamada, H.; Inotsume, S.; Kumagai, N.; Yamada, T.; Shimizu, M. Comparative Study of Boron Precursors for Chemical Vapor-Phase Deposition-Grown Hexagonal Boron Nitride Thin Films. *Phys. Status Solidi* **2021**, *218*, 2000241.
(5) Kim, K. S.; Kingston, C. T.; Hrdina, A.; Jakubinek, M. B.; Guan, J.; Plunkett, M.; Simard, B. Hydrogen-Catalyzed, Pilot-Scale Production of Small-Diameter Boron Nitride Nanotubes and Their Macroscopic Assemblies. *ACS Nano* **2014**, *8*, 6211−6220.
(6) Kim, K. S.; Couillard, M.; Shin, H.; Plunkett, M.; Ruth, D.; Kingston, C. T.; Simard, B. Role of Hydrogen in High-Yield Growth of Boron Nitride Nanotubes at Atmospheric Pressure by Induction Thermal Plasma. *ACS Nano* **2018**, *12*, 884−893.
(7) Kaganovich, I. Integrated Modeling of Carbon and Boron Nitride Nanotubes Synthesis in Plasma of High-Pressure Arc., In *APS Annual Gaseous Electronics Meeting Abstracts*, 2020; pp XF4-007.
(8) Smith, M. W.; Jordan, K. C.; Park, C.; Kim, J. W.; Lillehei, P. T.; Crooks, R.; Harrison, J. S. Very Long Single-and Few-Walled Boron Nitride Nanotubes via the Pressurized Vapor/Condenser Method. *Nanotechnology* **2009**, *20*, No. 505604.
(9) Fathalizadeh, A.; Pham, T.; Mickelson, W.; Zettl, A. Scaled Synthesis of Boron Nitride Nanotubes, Nanoribbons, and Nanococoons Using Direct Feedstock Injection into an Extended-Pressure, Inductively-Coupled Thermal Plasma. *Nano Lett.* **2014**, *14*, 4881−4886.
(10) Rao, R.; Pint, C. L.; Islam, A. E.; Weatherup, R. S.; Hofmann, S.; Meshot, E. R.; Wu, F.; Zhou, C.; Dee, N.; Amama, P. B.; et al. Carbon Nanotubes and Related Nanomaterials: Critical Advances and Challenges for Synthesis toward Mainstream Commercial Applications. *ACS Nano* **2018**, *12*, 11756−11784.
(11) Krstic, P.; Han, L. Can Hydrogen Catalyze Transitions between H-BN and c-BN in Volume Plasma? *J. Phys. Chem. C* **2018**, *122*, 936−944.
(12) Han, L.; Krstić, P. A Path for Synthesis of Boron-Nitride Nanostructures in Volume of Arc Plasma. *Nanotechnology* **2017**, *28*, No. 07LT01.
(13) Liu, S.; Van Duin, A. C. T.; Van Duin, D. M.; Liu, B.; Edgar, J. H. Atomistic Insights into Nucleation and Formation of Hexagonal Boron Nitride on Nickel from First-Principles-Based Reactive Molecular Dynamics Simulations. *ACS Nano* **2017**, *11*, 3585−3596.
(14) McLean, B. *Growth Mechanisms of Boron Nitride Nanotubes during Chemical Vapour Deposition*. Ph.D. thesis, 2020.
(15) Krstic, P. S.; Han, L.; Irle, S.; Nakai, H. Simulations of the Synthesis of Boron-Nitride Nanostructures in a Hot, High Pressure Gas Volume. *Chem. Sci.* **2018**, *9*, 3803−3819.
(16) Barsukov, Y.; Dwivedi, O.; Kaganovich, I.; Jubin, S.; Khrabry, A.; Ethier, S. Boron Nitride Nanotube Precursor Formation during High-Temperature Synthesis: Kinetic and Thermodynamic Modelling. *Nanotechnology* **2021**, *32*, 475604.
(17) Qian, H. J.; Van Duin, A. C. T.; Morokuma, K.; Irle, S. Reactive Molecular Dynamics Simulation of Fullerene Combustion Synthesis: ReaxFF vs DFTB Potentials. *J. Chem. Theory Comput.* **2011**, *7*, 2040−2048.
(18) Van Duin, A. C. T.; Dasgupta, S.; Lorant, F.; Goddard, W. A. ReaxFF: A Reactive Force Field for Hydrocarbons. *J. Phys. Chem. A* **2001**, *105*, 9396−9409.
(19) Chenoweth, K.; Van Duin, A. C. T.; Goddard, W. A. ReaxFF Reactive Force Field for Molecular Dynamics Simulations of Hydrocarbon Oxidation. *J. Phys. Chem. A* **2008**, *112*, 1040−1053.
(20) Johnston, H. S.; Parr, C. Activation Energies from Bond Energies. I. Hydrogen Transfer Reactions. *J. Am. Chem. Soc.* **1963**, *85*, 2544−2551.
(21) Mortier, W. J.; Ghosh, S. K.; Shankar, S. Electronegativity-Equalization Method for the Calculation of Atomic Charges in Molecules. *J. Am. Chem. Soc.* **1986**, *108*, 4315−4320.
(22) Senftle, T. P.; Hong, S.; Islam, M. M.; Kylasa, S. B.; Zheng, Y.; Shin, Y. K.; Junkermeier, C.; Engel-Herbert, R.; Janik, M. J.; Aktulga, H. M.; et al. The ReaxFF Reactive Force-Field: Development, Applications and Future Directions. *npj Comput. Mater.* **2016**, *2*, No. 15011.
(23) Chenoweth, K.; van Duin, A. C. T.; Goddard, W. A. ReaxFF Reactive Force Field for Molecular Dynamics Simulations of Hydrocarbon Oxidation. *J. Phys. Chem. A* **2008**, *112*, 1040.
(24) *AMS 2020.1, SCM, Theoretical Chemistry*; Vrije Universiteit: Amsterdam, The Netherlands, http://www.scm.com.
(25) Berendsen, H. J. C.; Postma, J. P. M.; van Gunsteren, W. F.; DiNola, A.; Haak, J. R. Molecular Dynamics with Coupling to an External Bath. *J. Chem. Phys.* **1984**, *81*, 3684−3690.
(26) Kwon, H.; Lele, A.; Zhu, J.; McEnally, C. S.; Pfefferle, L. D.; Xuan, Y.; van Duin, A. C. T. ReaxFF-Based Molecular Dynamics Study of Bio-Derived Polycyclic Alkanes as Potential Alternative Jet Fuels. *Fuel* **2020**, *279*, No. 118548.
(27) Lele, A.; Kwon, H.; Ganeshan, K.; Xuan, Y.; van Duin, A. C. T. ReaxFF Molecular Dynamics Study on Pyrolysis of Bicyclic Compounds for Aviation Fuel. *Fuel* **2021**, *297*, No. 120724.
(28) Bochevarov, A. D.; Harder, E.; Hughes, T. F.; Greenwood, J. R.; Braden, D. A.; Philipp, D. M.; Rinaldo, D.; Halls, M. D.; Zhang, J.; Friesner, R. A. Jaguar: A High-Performance Quantum Chemistry Software Program with Strengths in Life and Materials Sciences. *Int. J. Quantum Chem.* **2013**, *113*, 2110−2142.
(29) Beck, A. D. Density-Functional Thermochemistry. III. The Role of Exact Exchange. *J. Chem. Phys* **1993**, *98*, 5648.
(30) Krishnan, R.; Binkley, J. S.; Seeger, R.; Pople, J. A. Self-Consistent Molecular Orbital Methods. XX. A Basis Set for Correlated Wave Functions. *J. Chem. Phys.* **1980**, *72*, 650−654.
(31) Weismiller, M. R.; Duin, A. C. T. V.; Lee, J.; Yetter, R. A. ReaxFF Reactive Force Field Development and Applications for Molecular Dynamics Simulations of Ammonia Borane Dehydrogenation and Combustion. *J. Phys. Chem. A* **2010**, *114*, 5485−5492.
(32) Xuan, Y.; Jain, A.; Zafar, S.; Lotfi, R.; Nayir, N.; Wang, Y.; Choudhury, T. H.; Wright, S.; Feraca, J.; Rosenbaum, L.; et al. Multi-Scale Modeling of Gas-Phase Reactions in Metal-Organic Chemical Vapor Deposition Growth of WSe2. *J. Cryst. Growth* **2019**, *527*, No. 125247.
(33) Sun, B.; McKee, M. L. Computational Study of the Initial Stage of Diborane Pyrolysis. *Inorg. Chem.* **2013**, *52*, 5962−5969.
(34) Krep, L.; Kopp, W. A.; Kröger, L. C.; Döntgen, M.; Leonhard, K. Exploring the Chemistry of Low-Temperature Ignition by Pressure-Accelerated Dynamics. *ChemSystemsChem* **2020**, *2*, No. e1900043.
(35) Bansal, A.; Hilse, M.; Huet, B.; Wang, K.; Kozhakhmetov, A.; Kim, J. H.; Bachu, S.; Alem, N.; Collazo, R.; Robinson, J. A.; et al. Substrate Modification during Chemical Vapor Deposition of HBN on Sapphire. *ACS Appl. Mater. Interfaces* **2021**, *13*, 54516−54526.
(36) Ostwald, W. Z. Blocking of Ostwald Ripening Allowing Long-Term Stabilization. *Phys. Chem.* **1901**, *37*, 385.

https://doi.org/10.1021/acs.jpca.1c09648
J. Phys. Chem. A 2022, 126, 568−582

(37) Lifshitz, I. M.; Slyozov, V. V. The Kinetics of Precipitation from Supersaturated Solid Solutions. *J. Phys. Chem. Solids* **1961**, *19*, 35−50.
(38) Nishizawa, H.; Nishimura, Y.; Kobayashi, M.; Irle, S.; Nakai, H. Three Pillars for Achieving Quantum Mechanical Molecular Dynamics Simulations of Huge Systems: Divide-and-Conquer, Density-Functional Tight-Binding, and Massively Parallel Computation. *J. Comput. Chem.* **2016**, *37*, 1983−1992.

https://doi.org/10.1021/acs.jpca.1c09648
J. Phys. Chem. A 2022, 126, 568−582